

# Feedback Refined Local-Global Network for Super-Resolution of Hyperspectral Imagery

Zhenjie Tang, Qing Xu, Zhenwei Shi, Bin Pan

**Abstract**—With the development of deep learning technology, multi-spectral image super-resolution methods based on convolutional neural network have recently achieved great progress. However, the single hyperspectral image super-resolution remains a challenging problem due to the high-dimensional and complex spectral characteristics of hyperspectral data, which make it difficult to simultaneously capture spatial and spectral information. To deal with this issue, we propose a novel Feedback Refined Local-Global Network (FRLGN) for the super-resolution of hyperspectral image. To be specific, we develop a new Feedback Structure and a Local-Global Spectral Block to alleviate the difficulty in spatial and spectral feature extraction. The Feedback Structure can transfer the high-level information to guide the generation process of low-level feature, which is achieved by a recurrent structure with finite unfoldings. Furthermore, in order to effectively use the high-level information passed back, a Local-Global Spectral Block is constructed to handle the feedback connections. The Local-Global Spectral Block utilizes the feedback high-level information to correct the low-level feature from local spectral bands and generates powerful high-level representations among global spectral bands. By incorporating the Feedback Structure and Local-Global Spectral Block, the FRLGN can fully exploit spatial-spectral correlations among spectral bands and gradually reconstruct high-resolution hyperspectral images. The source code of FRLGN is available at <https://github.com/tangzhenjie/FRLGN>.

**Index Terms**—Hyperspectral image super-resolution, convolutional neural networks, feedback mechanism.

## I. INTRODUCTION

**H**YPERSPECTRAL imaging sensors collect and process information across different bands of the entire electromagnetic spectrum. Compared with multi-spectral image, the resulting hyperspectral image (HSI) contains richer spectral information and has been applied to resource management, target detection and land cover detection [1]–[4], etc. However, because of the limitation of imagery system, it is difficult to acquire an HSI with high spatial resolution. Therefore, how to

obtain a reliable high-resolution HSI is still a very challenging problem.

Recently, HSI super-resolution approaches have been intensively studied in remote sensing [5]. Based on the number of input images, the HSI super-resolution methods can be roughly divided into fusion-based HSI super-resolution [6]–[8] and single HSI super-resolution [9]–[11]. The fusion-based HSI super-resolution methods improves the spatial resolution by combining the observed low-resolution HSI with high-resolution multispectral image or panchromatic. For example, Wei *et al.* [12] introduced a variational-based approach to merge a high-resolution multispectral image with a low-resolution HSI. By considering the HSI as a 3D tensor, Wan *et al.* [13] designed a nonlocal 4-D tensor dictionary learning-based fusion approach. More recently, deep learning-based fusion methods have achieved excellent performance with the powerful representation capability of convolution neural network. For instance, Wei *et al.* [14] suggested using the deep neural network to capture plenty of HSI statistics and then putting these priors to regularize the super-resolution procedure of HSIs. Wei *et al.* [15] recently further designed a deep recursive residual network to probe the deep statistical prior information. Most fusion-based methods assume that the high-resolution auxiliary image is well co-registered with the low-resolution HSI. In real applications, it is difficult to obtain these co-registered auxiliary images, which hinders the progress of such technique.

By contrast, the single HSI super-resolution approaches do not need any auxiliary information and have better feasibility in practice, which only reconstruct the high-resolution HSI from a low-resolution HSI. To explore the spatial-spectral prior information of HSIs, some single HSI super-resolution methods based on dictionary learning, sparse representation and low-rank approximation have been proposed. For instance, Huang *et al.* [16] designed a noise-insensitive super-resolution mapping method based on multi-dictionary sparse representation. Wang *et al.* [17] introduced a new tensor-based approach to solve the HSI super-resolution problem by modeling three intrinsic characteristics of hyperspectral data. However, the hand-crafted priors can only reflect one aspect of the hyperspectral data, which make the reconstruction effect obvious only for the specified HSIs. In recent years, due to the success of deep learning technology in many fields, it has been applied to the single hyperspectral super-resolution task, and achieved satisfying super-resolution results [18]. For example, to alleviate spectral distortion, Hu *et al.* [19] designed a spectral difference convolutional network. Besides, Mei *et al.* [20] constructed a 3D super-resolution network to

This work was supported by the National Key R&D Program of China under the Grant 2019YFC1510905, the National Natural Science Foundation of China under the Grant 62001251 and 62001252 and the Scientific and Technological Research Project of Hebei Province Universities and Colleges under the Grant ZD2021311. (Corresponding author: Bin Pan.)

Zhenjie Tang is with the School of Civil Engineering, Tianjin University, Tianjin 300350, China (e-mail: tangzhenjie.hebut@gmail.com).

Qing Xu is with the College of Intelligence and Computing, Tianjin University, Tianjin 300350, China (e-mail: qingxu@tju.edu.cn). Zhenjie Tang and Qing Xu contributed equally to this manuscript.

Zhenwei Shi is with the Image Processing Center, School of Astronautics, Beihang University, Beijing 100191, China (e-mail: shizhenwei@buaa.edu.cn).

Bin Pan (Corresponding author) is with the School of Statistics and Data Science, Nankai University, Tianjin 300071, China (e-mail: pan-bin@nankai.edu.cn).

extract the prior information. Although the spectral correlation can be well exploited by 3D convolution operator, the amount of computation required by the model is very large. To solve the problem of high computation of 3D convolution, Jiang *et al.* [21] introduced a group convolution to explore the spatial information and the correlation among the spectral bands. Recently, Wang *et al.* [22] further designed a recurrent structure to investigate the spectral correlation among groups. Nonetheless, because of the high dimension and complex spectral patterns of hyperspectral data, it is hard to simultaneously explore the joint spatial and spectral information between continuous bands.

In this paper, in order to alleviate the difficulty of extracting spatial-spectral information from hyperspectral data, we propose a novel network for the single HSI super-resolution task, namely Feedback Refined Local-Global Network (FRLGN). FRLGN is motivated by the feedback mechanism [23], which can make the network transmit high-level semantic information back to the previous layers and refine these low-level feature representations. Recently, some researchers have adopted this feedback mechanism to design the network architecture for various vision tasks [24]–[26]. For instance, Han *et al.* [27] designed a two-state recurrent neural network, in which the information flows between two hidden states are exchanged in both directions. Taking advantage of the feedback mechanism to enhance the super-resolution results of HSIs, we designed a Feedback Structure (FS) and a Local-Global Spectral Block (LGSB) in FRLGN. To be specific, the Feedback Structure allows to use the feedback high-level information to correct the low-level representations through feedback connections. The FS is achieved by a recurrent structure with finite unfoldings. Furthermore, we construct a Local-Global Spectral Block to take full advantage of the feedback high-level information. The LGSB is composed of local and global spectral feature extraction layers, which can adjust the local spectral low-level representation input using the feedback high-level information and create a powerful high-level global spectral representation. The FRLGN is essentially a recurrent neural network with a Local-Global Spectral Block, which is specifically designed to explore the spatial and spectral prior of hyperspectral data. Experimental results indicate that LGSB is more suitable for HSI super-resolution task. Besides, in order to make the feedback high-level feature contains the high-resolution HSI information, we aggregate the losses of each iteration to optimize the network model. On the whole, the principle of the feedback mechanism is that the information of a coarse reconstructed HSI facilitates the low-resolution HSI to generate a better super-resolution HSI.

The main contributions of our work can be summarized as follows:

- A novel Feedback Refined Local-Global Network is proposed for the single HSI super-resolution task, which can effectively explore spatial-spectral priors between spectral bands.
- We construct a new Feedback Structure to correct the low-level representation using feedback high-level semantic information.
- We design a Local-Global Spectral Block to refine the lo-

cal spectral low-level representations using the feedback information, and then generate a more powerful global spectral high-level representation.

## II. PROPOSED METHOD

In this section, the detail description of FRLGN is first presented, and then the proposed Feedback Structure and Local-Global Spectral Block are introduced. At last, we interpret the loss function used in FRLGN approach.

### A. Network Architecture

As shown in Fig. 1, the FRLGN is unfolded to  $T$  iterations, where the order of each iteration  $t$  is from 1 to  $T$ . We link the losses of each iteration together so that the hidden state in FRLGN can contain the information of the high-resolution HSI. We describe the specific details of the loss function in the next Loss Function part. The sub-network in each iteration  $t$  consists of three Blocks: the Embedding Block, the Local-Global Spectral Block and the Reconstruction Block. Each iteration shares the weights of each block. For each iteration  $t$ , we also design a global skip connection that transmits an up-sampled HSI to the final output. Therefore, each iteration  $t$  of the sub-network is used to recover a residual image when a low-resolution HSI is input.

1) *The Embedding Block:* Different from the previous method of treating the HSI as a whole or multiple single-channel images, we divide the entire input low-resolution HSI into several groups. With this strategy, we can not only explore the correlation between adjacent spectral bands of the input HSI more easily, but also reduce the spectral dimension of the HSI. Specifically, the input low-resolution HSI  $I_{LR}$  is divided into  $G$  groups. More details are discussed in the experiment section. As shown in Fig. 1, for each group  $I_{LR}^g$ , we use one convolution operation to extract its shallow feature  $F_{EB}^g$ ,

$$I_{LR} = [I_{LR}^1, I_{LR}^2, I_{LR}^g, \dots, I_{LR}^G] \quad (1)$$

$$F_{EB}^g = f_{EB}(I_{LR}^g) \quad (2)$$

$$F_{EB} = [F_{EB}^1, F_{EB}^2, F_{EB}^g, \dots, F_{EB}^G] \quad (3)$$

where the  $f_{EB}$  denotes the operations of Embedding Block, eg., feature extraction layer for all groups. The  $[\ ]$  represents a cascading function. After that,  $F_{EB}$  is used as input to the Local-Global Spectral Block.

2) *The Local-Global Spectral Block:* For  $t$ -th iteration, Local-Global Spectral Block receives the the shallow feature  $F_{EB}$  and hidden state from past iteration  $F_{LGSB}^{t-1}$  through a feedback connection.  $F_{LGSB}^t$  denotes the result of LGSB. The mathematical formula of LGSB is as follows:

$$F_{LGSB}^t = f_{LGSB}(F_{LGSB}^{t-1}, F_{EB}) \quad (4)$$

where  $f_{LGSB}$  denotes the operations of the LGSB. More details of the LGSB can be found in Local-Global Spectral Block part.

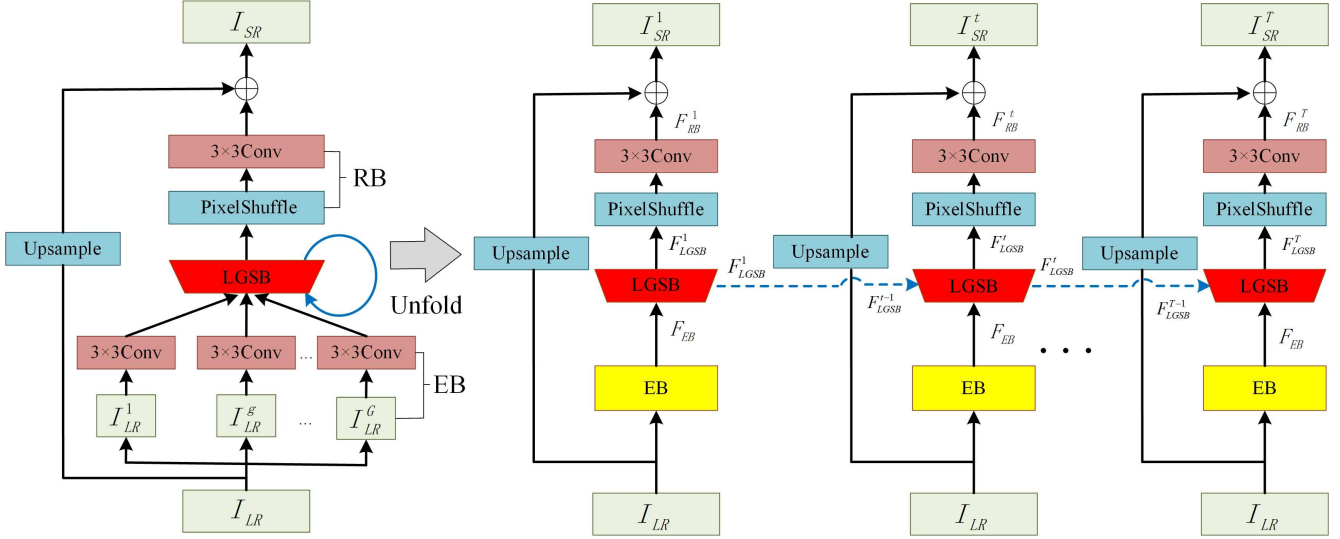


Fig. 1. The overview of our proposed Feedback Refined Local-Global Network (FRLGN). The blue arrows are the feedback connections and the Local-Global Spectral Block (LGSB) represented by the trapezoidal block is specifically designed for the task of super-resolution of hyperspectral images.

3) *The Reconstruction Block*: The reconstruction block firstly uses PixelShuffle [28] to upscale the feature  $F_{LGSB}^t$  to high-resolution one, and then a  $3 \times 3$  convolution operation is applied to create the residual image  $I_{Res}^t$ . The formula for reconstruction block is defined as:

$$I_{Res}^t = f_{RB}(F_{LGSB}^t) \quad (5)$$

where  $f_{RB}$  is the operation of the reconstruction block.

For the  $t$ -th iteration, the output super-resolution image  $I_{SR}^t$  is obtained by:

$$I_{SR}^t = I_{Res}^t + f_{UP}(I_{LR}) \quad (6)$$

where  $f_{UP}$  represents an upsampling operation. The choice of upsampling method is arbitrary. In this paper, we apply a Bicubic upsample approach. After  $T$  iterations, we will generate  $T$  super-resolution images  $(I_{SR}^1, I_{SR}^2, \dots, I_{SR}^T)$ .

### B. Feedback Structure

In HSI super-resolution task, some researchers [15], [22], [29] have made an effort to introduce the recurrent structure to improve super resolution results. However, in their network frameworks, the information flow from the low-resolution HSI to final super-resolution HSI is still feed-forward. As can be seen from Fig. 2(b), the recurrent structure adopted by these methods can be abstracted into a single-state recurrent network. These methods improve the feature representation of the model by running recursively on a specially designed network structure.

In this work, we design a Feedback Structure to reroute the output of the HSI super-resolution system to correct the input in each iteration. Fig. 2(a) illustrates the Feedback Structure of FRLGN. Specifically, the Local-Global Spectral Block receives the information of input low-resolution HSI and feedback high-level information from last iteration, then

generates coarse super-resolution result and high-level semantic guidance information for next iteration. The Feedback Structure can be characterized by:

$$I_{SR}^t = f_{FS}(I_{LR}, I_{SR}^{t-1}) \quad (7)$$

where the  $f_{FS}$  denotes the function of Feedback Structure.

### C. Local-Global Spectral Block

As an ill-posed problem, image super-resolution requires additional prior knowledge to regularize the reconstruction process. Traditional super-resolution methods usually make an effort to construct the regular terms of the super-resolution model, such as low-rank [30], total variation [31] and sparse [32], [33]. Whether the designed prior knowledge can characterize the observed HSI data directly determines the performance of the super-resolution method. Therefore, for the HSI super-resolution task, it is also essential to study the inherent characteristics of hyperspectral data, e.g., the spatial non-local self-similarity and the high-correlation among spectral bands [34]. However, the manually designed constraints are not enough to achieve accurate restoration of HSIs.

In this work, a novel Local-Global Spectral Block is introduced to exploit the spatial-spectral prior with the help of feedback high-level semantic information from hidden state. As can be seen in Fig. 3(a), for iteration  $t$ , the LGSB inputs the feedback global spectral high-level information  $F_{LGSB}^{t-1}$  to correct the  $G$  groups local spectral low-level representations,  $F_{EB} = [F_{EB}^1, F_{EB}^2, F_{EB}^g, \dots, F_{EB}^G]$ , and then creates more effective high-level feature  $F_{LGSB}^t$  for the next iteration and the reconstruction block. The LGSB contains  $G$  groups local spectral feature extraction layers and one global spectral feature extraction layer. For simplicity, we use  $Conv(k)$  and  $Deconv(k)$  to denote a convolution operation and a deconvolutional operation, where the  $k$  represents the size of convolution kernel.

At the beginning of the LGSB, the downsampled  $F_{LGSB}^{t-1}$  and each group  $F_{EB}^g$  are concatenated and compressed by one

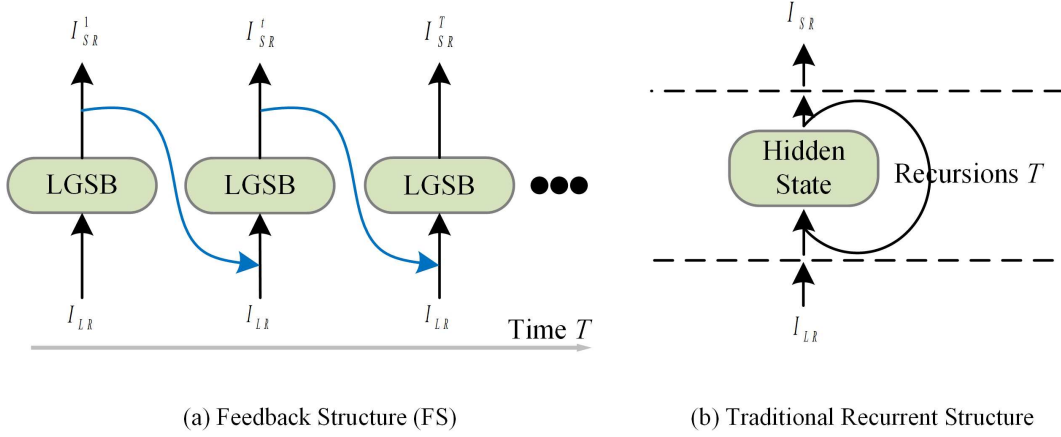


Fig. 2. (a) The illustration of the Feedback Structure (FS) in the proposed FRLGN network and the blue arrow is the feedback connection. (b) The architecture of Traditional Recurrent Structure.

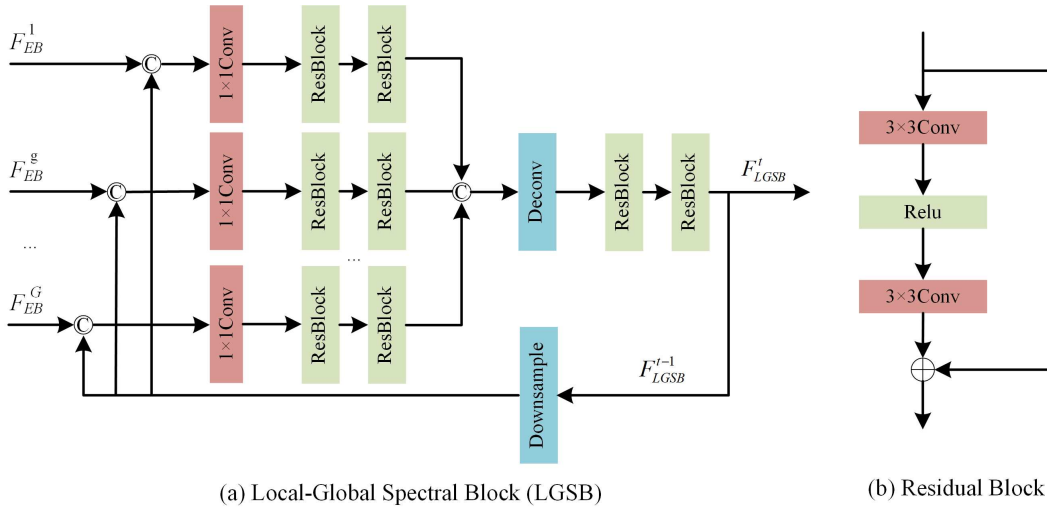


Fig. 3. The network architecture of the Local-Global Spectral Block (LGSB): (a) the Local-Global Spectral Block, (b) the Residual Block

$Conv(1)$  operation to refine the input each group feature  $F_{EB}^g$  by feedback information  $F_{LGSB}^{t-1}$ , producing the refined group feature  $F_g^t$ .

$$F_g^t = f_{Com}([f_{Down}(F_{LGSB}^{t-1}), F_{EB}^g]) \quad (8)$$

where  $f_{Down}$  refers to downsample operation using average pooling with a kernel of 2 and stride of 2. The  $[f_{Down}(F_{LGSB}^{t-1}), F_{EB}^g]$  refers to the concatenation of  $f_{Down}(F_{LGSB}^{t-1})$  and  $F_{EB}^g$ . The  $f_{Com}$  denotes the initial compression operation.

After obtaining the refined group feature  $F_g^t$ , we add a local spectral feature extraction layer to explore the local spectral correlation, which consists of two residual blocks as shown in Fig. 3(b). Let  $L_g^t$  be the  $g$ -th group local spectral LR feature map.  $L_g^t$  can be obtained by:

$$L_g^t = f_{Local}(F_g^t) \quad (9)$$

where the  $f_{Local}$  denotes local spectral feature extraction layer.

After that, we pass all the local spectral LR feature maps to the global spectral feature extraction layer, which contains

one upsample  $Deconv(2)$  operation and two residual blocks. Note that we propose a strategy of progressive super-resolution reconstruction to stabilize the training process. Particularly, in addition to the reconstruction block, we also add an upsampling operation in the global spectral feature extraction layer. At last, the global spectral high-level feature  $F_{LGSB}^t$  can be obtained by:

$$F_{LGSB}^t = f_{Global}([L_1^t, L_2^t, \dots, L_G^t]) \quad (10)$$

where the  $f_{Global}$  denotes the the global spectral feature extraction layer.

#### D. Loss Function

To optimize the FRLGN, we choose the most commonly used  $L1$  loss function to measure the HSI reconstruction performance. Finally, the output result of FRLGN is the weighted average of all intermediate super-resolution results:

$$I_{SR} = \frac{1}{T} \sum_{t=1}^T I_{Res}^t + f_{UP}(I_{LR}) \quad (11)$$

The loss function of FRLGN is determined by:

$$L(\Theta) = \|I_{HR} - I_{SR}\|_1 \quad (12)$$

where the  $\Theta$  represents the parameters of our proposed FRLGN and the  $I_{HR}$  is the corresponding target high-resolution HSI. The training procedure of FRLGN is shown in Algorithm 1.

---

**Algorithm 1: Training Process of FRLGN**


---

**input :** Low-resolution HSI  $I_{LR}$ ;  
 High-resolution HSI  $I_{HR}$ ;  
 The number of iterations  $T$ ;  
 The number of local spectral groups in LGSB

G.

**output:** Super-resolution HSI  $I_{SR}$

**repeat**

  Initialization:

$$I_{LR} = \{I_{LR}^1, I_{LR}^2, \dots, I_{LR}^G\};$$

$$F_{LGSB}^0 = \text{None};$$

  Shallow feature extraction by the Embedding

  Block:

$$F_{EB} = f_{EB}(I_{LR});$$

$T$  intermediate prediction result generation by the

  Local-Global Spectral Block and the

  Reconstruction Block:

**for**  $t = 1$  to  $T$  **do**

$$F_{LGSB}^t = f_{LGSB}(F_{LGSB}^{t-1}, F_{EB});$$

$$I_{Res}^t = f_{RB}(F_{LGSB}^t)$$

**end**

  Final output:

$$I_{SR} = \frac{1}{T} \sum_{t=1}^T I_{Res}^t + f_{UP}(I_{LR})$$

  Update the FRLGN network parameters by minimizing the loss between the reconstructed  $I_{SR}$  and the corresponding label  $I_{HR}$

**until** convergence;

---

### III. EXPERIMENTS AND RESULTS

#### A. Datasets

1) *CAVE dataset*: The CAVE dataset [35] is a HSI dataset of real-world materials and objects, which are captured by a Cooled CCD camera. The hyperspectral camera collects information from the 400nm-700nm spectral range in 10 nm steps. This dataset consists of 32 HSIs with a size of  $512 \times 512 \times 31$  pixels, which are further divided into 5 groups, namely food and drinks, skin and hair, paints, real and fake, and stuff.

2) *Harvard dataset*: The Harvard dataset [36] contains 77 HSIs of  $1040 \times 1392 \times 31$  size from outdoor and indoor scenes. These HSIs are captured by a commercial hyperspectral camera, which collects the spectral data in 10 nm steps over the wavelength range of 400 nm to 700 nm.

3) *Chikusei dataset*: The Chikusei dataset [37] consists of  $2517 \times 2335$  pixels with a spatial resolution of 2.5 m. The dataset was taken by an airborne hyperspectral imaging sensor in the agricultural and urban areas of Chikusai, Japan. This dataset captures 128 spectral bands from the 363 nm to 1018

nm. Since the lack of edge information, we first cut the original HSI to generate an image of  $2304 \times 2048 \times 128$  pixels and then the generated image is further split into a training set and a test set. In particular, we first extract the top region of the generated image to create the test set, which consists of four HSIs with a pixel size of  $512 \times 512 \times 128$  that do not overlap each other. And the remaining region of the generated image is used as training data.

#### B. Implementation Details

Since HSIs are collected by different hyperspectral imaging sensors, HSI datasets tend to have different numbers of spectral channels. Therefore, we need to learn a super-resolution HSI model separately for each HSI dataset. In the next experiments, 80% of samples in the dataset are used to train the super-resolution models and the remaining samples are utilized for testing.

During training, 12 randomly selected patches are fed to the FRLGN network. To obtain low-resolution HSIs, we down-sample these patches to  $32 \times 32 \times L$  pixels based on the scale factor  $s$ . Furthermore, we use the bicubic interpolation function to down-sample these patches. In our network, the convolution operators with a kernel 3 adopt a zero-padding strategy to ensure that the intermediate features have the same spatial size. We up-sample the resulting features by a factor of 2 using a deconvolution with a kernel 2 and a stride 2. The ADAM [38] with an initial learning rate of  $2e-4$  is used to optimize the FRLGN network.

At the testing stage, in order to improve testing efficiency, we use only the  $512 \times 512$  area in the upper left corner of test HSIs for evaluation. In this work, the Pytorch library is used to implement and train our proposed FRLGN network.

#### C. Evaluation Metrics

In this section, we choose six commonly used quantitative metrics to evaluate the performance of FRLGN, i.e., cross correlation (CC) [39], spectral angle mapper (SAM) [40], root mean squared error (RMSE), the erreur relative globale adimensionnelle de synthese (ERGAS) [41], peak signal-to-noise ratio (PSNR) and structure similarity (SSIM) [42]. As the CC, RMSE, PSNR and SSIM are widely used quantitative metrics in HSI super-resolution tasks, we omit their detailed description here. In addition, ERGAS performs a global statistical measure on the reconstructed HSIs, which is calculated by

$$ERGAS(I_{HR}, I_{SR}) = 100s \sqrt{\frac{1}{L} \sum_{l=1}^L \left( \frac{RMSE_l}{\mu_l} \right)^2} \quad (13)$$

in which  $RMSE_l = (\|I_{SR}^l - I_{HR}^l\|_F / \sqrt{n})$ . Here,  $n$  and  $\mu_l$  represent the number of spatial pixels and mean of the  $l$ th band from the ground truth  $I_{HR}$ , respectively. The  $I_{SR}^l$  and  $I_{HR}^l$  denote the  $l$ th band of  $I_{SR}$  and  $I_{HR}$ , respectively. SAM is used to evaluate the preservation of spectral band information for each spatial location of the HSI. SAM is obtained by calculating the angle between two spectral vectors from the

TABLE I  
CONVERGENCE ANALYSIS OF  $T$  WHEN  $G=8$

$T$	1	2	3	4	5	6
PSNR(dB)	37.0815	37.5073	37.7574	37.8131	37.8639	37.8905

TABLE II  
CONVERGENCE ANALYSIS OF  $G$  WHEN  $T=6$

$G$	1	2	4	8
SAM	3.5977	3.5276	3.4792	3.4332

same spatial position of  $I_{SR}$  and  $I_{HR}$ . The formula of SAM is presented as

$$SAM(\mathbf{x}, \hat{\mathbf{x}}) = \arccos\left(\frac{\langle \mathbf{x}, \hat{\mathbf{x}} \rangle}{\|\mathbf{x}\|_2 \|\hat{\mathbf{x}}\|_2}\right) \quad (14)$$

in which  $\hat{\mathbf{x}}$  and  $\mathbf{x}$  denote the two spectral vectors from  $I_{SR}$  and  $I_{HR}$ , respectively. And the  $\langle \cdot, \cdot \rangle$  is the dot product of two vectors,  $\|\mathbf{x}\|_2$  represent the  $l_2$  regularization operation of a vector. For PSNR and SSIM, we present the average metric values of all spectral bands. The best values for CC, SAM, RMSE, ERGAS, PSNR, SSIM are 1, 0, 0, 0,  $+\infty$ , and 1, respectively.

#### D. Study of $T$ and $G$

In this part, we discussed the effect of iterations (denoted as  $T$ ) and local spectral groups (denoted as  $G$ ) in the Local-Global Spectral Block on the FRLGN performance on the CAVE dataset. In subsequent experiments, we set the base number of filters to 256. By fixing  $G$  to 8, we first explore the influence of  $T$  on HSI reconstruction. Table I shows that the super-resolution performance is improved with the help of feedback connections compared to the network without feedback connections ( $T=1$ ). Moreover, the quality of reconstruction has been further improved as the increasing iteration  $T$ . On the other hand, it also indicates that our proposed Local-Global Spectral Block would certainly benefit from cross-time feedback information. After that, we also discuss the influence of  $G$  by fixing the  $T$  to 6. From Table II, we can observe that with the help of local-spectral grouping strategy, the spectrum reconstruction performance is enhanced compared to the network without the grouping strategy ( $G=1$ ). In addition, with the increase of  $G$ , the spectral representation of FRLGN becomes more powerful and the spectral reconstruction quality is also improved. In a word, choosing larger  $T$  or  $G$  can obtain better super-resolution results. In next experiments, we set  $T=6$ ,  $G=8$  for CAVE dataset and Harvard dataset, and  $T=6$ ,  $G=12$  for Chikusei dataset.

#### E. Comparisons with the State-of-the-Art Methods

In this section, we evaluate the single image super-resolution effect of FRLGN in detail on three benchmarks, namely CAVE dataset [35], Harvard dataset [36] and Chikusei dataset [37].

TABLE III  
QUANTITATIVE ANALYSIS OF SEVEN DIFFERENT COMPARISON METHODS ON CAVE TEST DATASET INVOLVING SIX METRICS.

	$s$	CC $\uparrow$	SAM $\downarrow$	RMSE $\downarrow$	ERGAS $\downarrow$	PSNR $\uparrow$	SSIM $\uparrow$
Bicubic	4	0.9846	5.1832	0.0224	7.7384	34.5069	0.9472
VDSR [43]	4	0.9896	4.3622	0.0188	6.3067	36.1348	0.9612
RCAN [44]	4	0.9913	4.3058	0.0172	5.7796	36.7979	0.9657
3DCNN [20]	4	0.9862	4.2297	0.0212	7.3182	34.9853	0.9549
GDRRN [29]	4	0.9891	4.2970	0.0192	6.5087	35.8465	0.9594
SSPSR [21]	4	0.9915	3.7384	0.0168	5.7527	37.0479	0.9682
FRLGN	4	<b>0.9930</b>	<b>3.4332</b>	<b>0.0152</b>	<b>5.1599</b>	<b>37.8905</b>	<b>0.9737</b>
Bicubic	8	0.9564	7.3210	0.0385	12.8323	29.5763	0.8741
VDSR [43]	8	0.9615	5.8692	0.0369	12.0527	30.0080	0.8999
RCAN [44]	8	0.9671	5.9008	0.0340	11.1373	30.7372	0.9061
3DCNN [20]	8	0.9594	5.6079	0.0370	12.3341	29.8880	0.8961
GDRRN [29]	8	0.9611	5.8864	0.0368	12.0684	30.0042	0.8966
SSPSR [21]	8	0.9675	5.6617	0.0341	11.0506	30.7976	0.9098
FRLGN	8	<b>0.9712</b>	<b>5.0550</b>	<b>0.0323</b>	<b>10.3982</b>	<b>31.4007</b>	<b>0.9159</b>

TABLE IV  
QUANTITATIVE ANALYSIS OF SEVEN DIFFERENT COMPARISON METHODS ON HARVARD TEST DATASET INVOLVING SIX METRICS.

	$s$	CC $\uparrow$	SAM $\downarrow$	RMSE $\downarrow$	ERGAS $\downarrow$	PSNR $\uparrow$	SSIM $\uparrow$
Bicubic	4	0.9606	2.5671	0.0101	3.0957	43.9037	0.9582
VDSR [43]	4	0.9640	2.5709	0.0090	2.8602	44.6486	0.9634
RCAN [44]	4	0.9671	2.4097	0.0086	2.7537	45.1204	0.9663
3DCNN [20]	4	0.9614	2.3917	0.0098	3.0324	44.1815	0.9600
GDRRN [29]	4	0.9630	2.4924	0.0093	2.9276	44.4577	0.9620
SSPSR [21]	4	0.9704	2.2766	0.0082	2.5893	45.5460	0.9684
FRLGN	4	<b>0.9722</b>	<b>2.2496</b>	<b>0.0074</b>	<b>2.4463</b>	<b>46.1866</b>	<b>0.9730</b>
Bicubic	8	0.9098	3.0165	0.0179	5.0694	39.6681	0.9131
VDSR [43]	8	0.9185	3.0093	0.0165	4.7369	40.2490	0.9223
RCAN [44]	8	0.9312	2.7808	0.0150	4.3438	40.9853	<u>0.9313</u>
3DCNN [20]	8	0.9128	2.7853	0.0172	4.9422	39.9615	0.9175
GDRRN [29]	8	0.9175	2.8669	0.0166	4.7946	40.1831	0.9214
SSPSR [21]	8	0.9338	<b>2.6202</b>	0.0149	4.2458	41.1869	0.9313
FRLGN	8	<b>0.9373</b>	2.7665	<b>0.0139</b>	<b>4.0316</b>	<b>41.6320</b>	<b>0.9374</b>

TABLE V  
QUANTITATIVE ANALYSIS OF SEVEN DIFFERENT COMPARISON METHODS ON CHIKUSEI TEST DATASET INVOLVING SIX METRICS.

	$s$	CC $\uparrow$	SAM $\downarrow$	RMSE $\downarrow$	ERGAS $\downarrow$	PSNR $\uparrow$	SSIM $\uparrow$
Bicubic	4	0.8987	3.7666	0.0176	7.6532	36.5603	0.8882
VDSR [43]	4	0.9176	3.1003	0.0155	6.9534	37.5648	0.9113
RCAN [44]	4	0.9142	3.0936	0.0156	7.1099	37.4313	0.9104
3DCNN [20]	4	0.9047	3.4808	0.0169	7.3419	36.9090	0.8931
GDRRN [29]	4	0.9144	3.2178	0.0159	7.0426	37.3754	0.9060
SSPSR [21]	4	0.9250	2.8281	0.0148	6.6082	37.9698	0.9193
FRLGN	4	<b>0.9283</b>	<b>2.7580</b>	<b>0.0143</b>	<b>6.4953</b>	<b>38.2085</b>	<b>0.9240</b>
Bicubic	8	0.7546	5.9617	0.0274	11.9665	32.7047	0.7829
VDSR [43]	8	0.7840	5.3103	0.0250	10.9097	33.4964	0.8069
RCAN [44]	8	0.7630	6.5447	0.0258	11.9078	33.0475	0.7946
3DCNN [20]	8	0.7723	5.5506	0.0257	11.0971	33.3107	0.7955
GDRRN [29]	8	0.7842	5.3033	0.0249	10.9107	33.5236	0.8062
SSPSR [21]	8	0.7880	5.2415	0.0247	<b>10.7863</b>	33.6194	0.8106
FRLGN	8	<b>0.7887</b>	<b>5.2122</b>	<b>0.0246</b>	10.8033	<b>33.6332</b>	<b>0.8145</b>

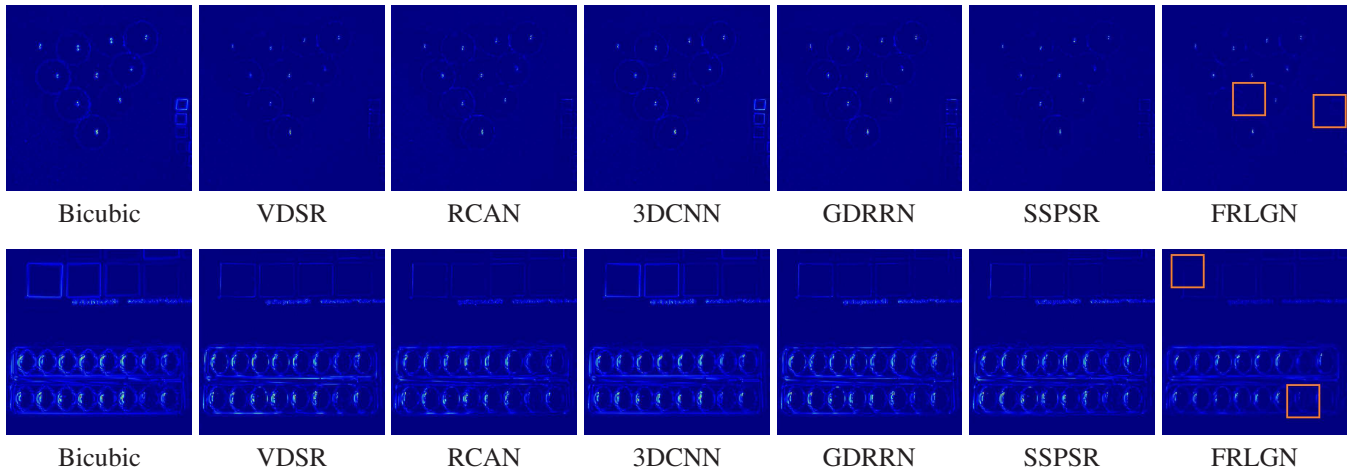


Fig. 4. Mean error maps of superballs and paints hyperspectral images from the CAVE testing dataset with a scale factor of 4

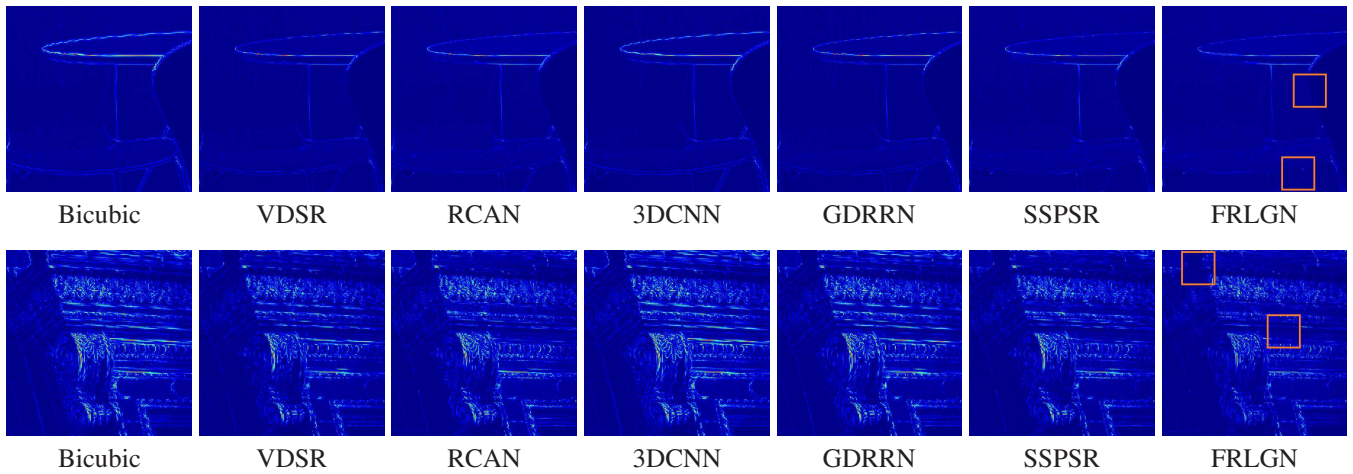


Fig. 5. Mean error maps of two hyperspectral images from the Harvard testing dataset with the scale factor 4.

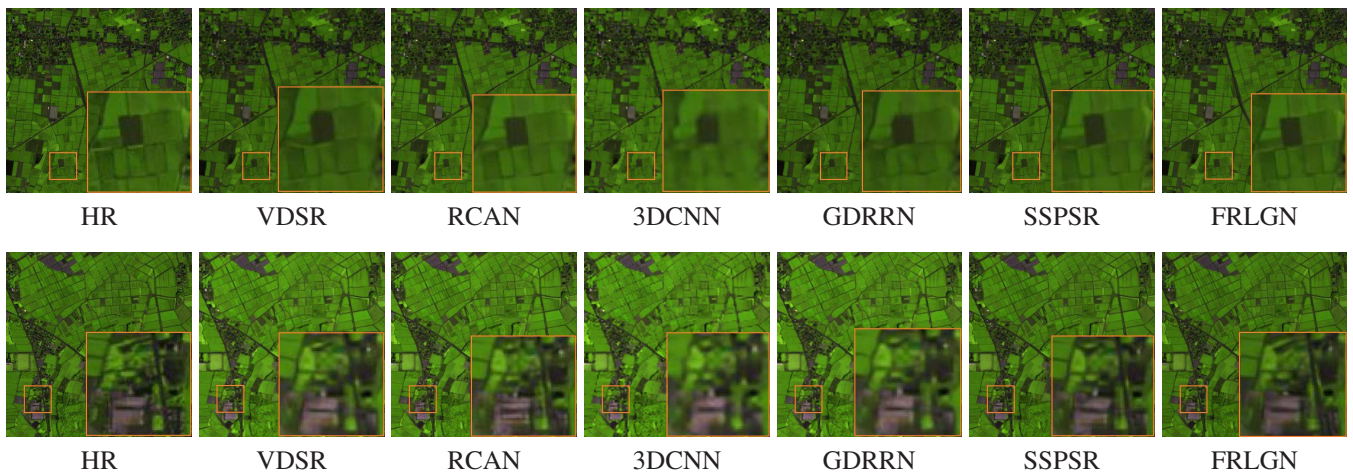


Fig. 6. Two reconstructed hyperspectral images from the Chikusei testing dataset with the scale factor 4, in which the bands 70-100-36 is treat as R-G-B.

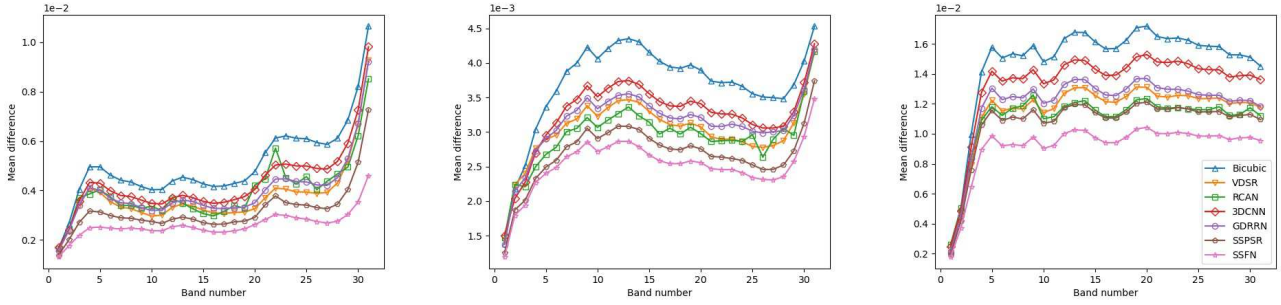


Fig. 7. Mean spectral difference curve of three hyperspectral images from the CAVE testing dataset with the scale factor 4:superballs,sushi,chart\_and\_stuffed.

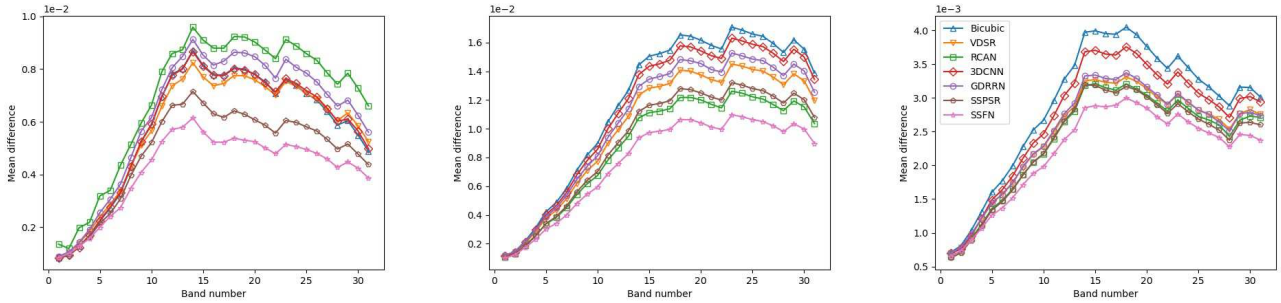


Fig. 8. Mean spectral difference curve of three hyperspectral images from the Harvard testing dataset with the scale factor 4.

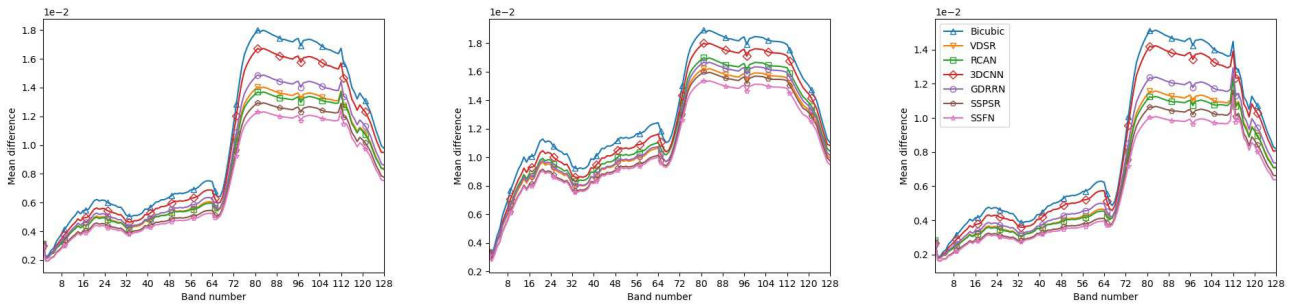


Fig. 9. Mean spectral difference curve of three hyperspectral images from the Chikusei testing dataset with the scale factor 4.

Specifically, we compare the FRLGN with five existing super-resolution approaches, including two advanced deep multispectral image super-resolution methods, VDSR [43], RCAN [44], and three representative HSI super-resolution methods, 3DCNN [20], GDRRN [29] and SSFSR [21]. In addition, we carefully tune the hyper-parameters of these super-resolution methods to obtain a good performance. Moreover, the bicubic interpolation is used as our baseline model. Table III, IV and V depict the quantitative performance of all super-resolution algorithms over testing images on three datasets, where bold indicates the best results.

Table III shows that our FRLGN method outperforms other comparative methods in all objective assessment metrics. Specifically, the baseline approach has the worst performance among these compared algorithms. As the competitive multispectral image super-resolution methods, VDSR and RCAN can generate very satisfactory results. Nonetheless, in compar-

ison with those HSI super-resolution methods, *i.e.*, 3DCNN [20] and SSFSR [21], their spectral reconstruction effect (SAM) is relatively poor. This indicates that the multispectral super-resolution approaches cannot effectively explore the spectral prior information from the hyperspectral data. Similar to our work, SSFSR [21] also adopts a group strategy but neglects the continuous relationship among band groups. Therefore, it achieves the suboptimal results for the SAM indices. Compared with other comparison SR methods, our proposed FRLGN can obtain better performance in spectral and spatial dimensions. In term of PSNR, the FRLGN was 0.8 and 0.6 higher than the suboptimal method for upsampling factors  $d$  of 4 and 8, respectively. The table IV and V show the similar results. In conclusion, FRLGN has presented advantages on three datasets compared to existing SR methods, especially for PSNR and SSIM.

In order to further prove the effectiveness of FRLGN,

Fig. 4 and 5 display the mean absolute error maps across all spectral bands of two HSIs with the scale factor  $\times 4$  from the CAVE testing dataset and Harvard testing dataset, respectively. Principally, the bluer the color of the error map, the better the reconstructed HSI. From fig. 4 and 5, we can easily discover that the FRLGN method can obtain better reconstruction fidelity when restoring the spatial information of the original HSI. Specifically, in contrast to with the suboptimal SSPSR method, FRLGN performs better in reconstructing textures such as edges and structures. Besides, we also display two reconstructed high-resolution HSIs from Chikusei test dataset with a downsampling factor of 4 in Fig. 6. As can be seen from Fig. 6, our FRLGN can restore finer texture details than other comparison methods.

In addition, to prove our advantage in reconstructing spectral information, Fig. 7, 8 and 9 show the average absolute difference of all comparison methods along the spectral dimension. The average spectral error curve has a better visualization effect than displaying the spectral reflectance of multiple locations. As shown in Fig. 7, 8 and 9, our method has the lowest average spectral error curve, which indicates that FRLGN has better spectral reconstruction ability. This can be attributed to the guidance of the global spectral feedback information to the local spectral band group. Moreover, as iterations increase, the local spectral group information gradually accumulates, leading to better spectral reconstruction performance.

#### IV. CONCLUSION

Considering the difficulty of simultaneously exploring the spatial and spectral information of hyperspectral data, we propose a new approach for the single HSI super-resolution task, called Feedback Refined Local-Global Network. FRLGN can produce a clear high-resolution HSI by introducing a Feedback Structure and a Local-Global Spectral Block. In particular, we construct a recurrent neural network with feedback connections to refine low-level feature representations using feedback global spectral high-level semantic information. Furthermore, taking advantage of the feedback high-level semantic information, we carefully design a Local-Global Spectral Block to guide the extraction process of low-level representations between local spectral bands using the feedback information, and then generate a more powerful high-level feature among global spectral bands. With the increasing number of iterations, the spatial-spectral prior gradually accumulates, leading to better HSI reconstruction performance. The comprehensive experimental results and visual data analysis show the effectiveness of the proposed FRLGN.

#### REFERENCES

- [1] Z. Zou and Z. Shi, "Hierarchical suppression method for hyperspectral target detection," *IEEE Transactions on Geoscience and Remote Sensing*, vol. 54, no. 1, pp. 330–342, 2016.
- [2] Z. Shao, L. Zhang, X. Zhou, and L. Ding, "A novel hierarchical semisupervised svm for classification of hyperspectral images," *IEEE Geoscience and Remote Sensing Letters*, vol. 11, no. 9, pp. 1609–1613, 2014.
- [3] Q. Wang, Z. Yuan, Q. Du, and X. Li, "Getnet: A general end-to-end 2-d cnn framework for hyperspectral image change detection," *IEEE Transactions on Geoscience and Remote Sensing*, vol. 57, no. 1, pp. 3–13, 2019.
- [4] C. Yan, X. Bai, P. Ren, L. Bai, W. Tang, and J. Zhou, "Band weighting via maximizing interclass distance for hyperspectral image classification," *IEEE Geoscience and Remote Sensing Letters*, vol. 13, no. 7, pp. 922–925, 2016.
- [5] Q. Li, Q. Wang, and X. Li, "Exploring the relationship between 2d/3d convolution for hyperspectral image super-resolution," *IEEE Transactions on Geoscience and Remote Sensing*, vol. 59, no. 10, pp. 8693–8703, 2021.
- [6] H. Gao, G. Zhang, and M. Huang, "Hyperspectral image superresolution via structure-tensor-based image matting," *IEEE Journal of Selected Topics in Applied Earth Observations and Remote Sensing*, vol. 14, pp. 7994–8007, 2021.
- [7] W. Sun, K. Ren, X. Meng, C. Xiao, G. Yang, and J. Peng, "A band divide-and-conquer multispectral and hyperspectral image fusion method," *IEEE Transactions on Geoscience and Remote Sensing*, vol. 60, pp. 1–13, 2022.
- [8] W. Chen, X. Zheng, and X. Lu, "Hyperspectral image super-resolution via self-supervised spectral-spatial residual network," *Remote Sensing*, vol. 13, no. 7, p. 1260, 2021.
- [9] Y. Fu, Z. Liang, and S. You, "Bidirectional 3d quasi-recurrent neural network for hyperspectral image super-resolution," *IEEE Journal of Selected Topics in Applied Earth Observations and Remote Sensing*, vol. 14, pp. 2674–2688, 2021.
- [10] D. Liu, J. Li, and Q. Yuan, "A spectral grouping and attention-driven residual dense network for hyperspectral image super-resolution," *IEEE Transactions on Geoscience and Remote Sensing*, vol. 59, no. 9, pp. 7711–7725, 2021.
- [11] X. Wang, J. Ma, J. Jiang, and X.-P. Zhang, "Dilated projection correction network based on autoencoder for hyperspectral image super-resolution," *Neural Networks*, vol. 146, pp. 107–119, 2022.
- [12] Q. Wei, J. Bioucas-Dias, N. Dobigeon, and J.-Y. Tourneret, "Hyperspectral and multispectral image fusion based on a sparse representation," *IEEE Transactions on Geoscience and Remote Sensing*, vol. 53, no. 7, pp. 3658–3668, 2015.
- [13] W. Wan, W. Guo, H. Huang, and J. Liu, "Nonnegative and nonlocal sparse tensor factorization-based hyperspectral image super-resolution," *IEEE Transactions on Geoscience and Remote Sensing*, vol. 58, no. 12, pp. 8384–8394, 2020.
- [14] W. Wei, J. Nie, L. Zhang, and Y. Zhang, "Unsupervised recurrent hyperspectral imagery super-resolution using pixel-aware refinement," *IEEE Transactions on Geoscience and Remote Sensing*, vol. 60, pp. 1–15, 2022.
- [15] W. Wei, J. Nie, Y. Li, L. Zhang, and Y. Zhang, "Deep recursive network for hyperspectral image super-resolution," *IEEE Transactions on Computational Imaging*, vol. 6, pp. 1233–1244, 2020.
- [16] H. Huang, J. Yu, and W. Sun, "Super-resolution mapping via multi-dictionary based sparse representation," in *2014 IEEE International Conference on Acoustics, Speech and Signal Processing (ICASSP)*, 2014, pp. 3523–3527.
- [17] W. Yao, C. Xi, H. Zhi, and H. Shiyong, "Hyperspectral image super-resolution via nonlocal low-rank tensor approximation and total variation regularization," *Remote Sensing*, vol. 9, no. 12, p. 1286, 2017.
- [18] B. Pan, Q. Qu, X. Xu, and Z. Shi, "Structure-color preserving network for hyperspectral image super resolution," *IEEE Transactions on Geoscience and Remote Sensing*, 2021.
- [19] J. Hu, Y. Li, and W. Xie, "Hyperspectral image super-resolution by spectral difference learning and spatial error correction," *IEEE Geoscience and Remote Sensing Letters*, vol. 14, no. 10, pp. 1825–1829, 2017.
- [20] S. Mei, X. Yuan, J. Ji, Y. Zhang, S. Wan, and Q. Du, "Hyperspectral image spatial super-resolution via 3d full convolutional neural network," *Remote Sensing*, vol. 9, no. 11, p. 1139, 2017.
- [21] J. Jiang, H. Sun, X. Liu, and J. Ma, "Learning spatial-spectral prior for super-resolution of hyperspectral imagery," *IEEE Transactions on Computational Imaging*, vol. 6, pp. 1082–1096, 2020.
- [22] X. Wang, J. Ma, and J. Jiang, "Hyperspectral image super-resolution via recurrent feedback embedding and spatial-spectral consistency regularization," *IEEE Transactions on Geoscience and Remote Sensing*, vol. 60, pp. 1–13, 2022.
- [23] J. Hupé, A. James, B. Payne, S. Lomber, P. Girard, and J. Bullier, "Cortical feedback improves discrimination between figure and background by v1, v2 and v3 neurons," *Nature*, vol. 394, no. 6695, pp. 784–787, 1998.
- [24] C. Cao, X. Liu, Y. Yang, Y. Yu, J. Wang, Z. Wang, Y. Huang, L. Wang, C. Huang, W. Xu *et al.*, "Look and think twice: Capturing top-down visual attention with feedback convolutional neural networks," in *Proceedings of the IEEE international conference on computer vision*, 2015, pp. 2956–2964.

- [25] J. Carreira, P. Agrawal, K. Fragkiadaki, and J. Malik, "Human pose estimation with iterative error feedback," in *Proceedings of the IEEE conference on computer vision and pattern recognition*, 2016, pp. 4733–4742.
- [26] Z. Li, J. Yang, Z. Liu, X. Yang, G. Jeon, and W. Wu, "Feedback network for image super-resolution," in *Proceedings of the IEEE/CVF Conference on Computer Vision and Pattern Recognition*, 2019, pp. 3867–3876.
- [27] W. Han, S. Chang, D. Liu, M. Yu, M. Witbrock, and T. S. Huang, "Image super-resolution via dual-state recurrent networks," in *Proceedings of the IEEE conference on computer vision and pattern recognition*, 2018, pp. 1654–1663.
- [28] W. Shi, J. Caballero, F. Huszár, J. Totz, A. P. Aitken, R. Bishop, D. Rueckert, and Z. Wang, "Real-time single image and video super-resolution using an efficient sub-pixel convolutional neural network," in *Proceedings of the IEEE conference on computer vision and pattern recognition*, 2016, pp. 1874–1883.
- [29] Y. Li, L. Zhang, C. Dingli, W. Wei, and Y. Zhang, "Single hyperspectral image super-resolution with grouped deep recursive residual network," in *2018 IEEE Fourth International Conference on Multimedia Big Data (BigMM)*. IEEE, 2018, pp. 1–4.
- [30] R. Dian and S. Li, "Hyperspectral image super-resolution via subspace-based low tensor multi-rank regularization," *IEEE Transactions on Image Processing*, vol. 28, no. 10, pp. 5135–5146, 2019.
- [31] S. He, H. Zhou, Y. Wang, W. Cao, and Z. Han, "Super-resolution reconstruction of hyperspectral images via low rank tensor modeling and total variation regularization," in *2016 IEEE International Geoscience and Remote Sensing Symposium (IGARSS)*. IEEE, 2016, pp. 6962–6965.
- [32] Y. Xu, Z. Wu, J. Chanussot, and Z. Wei, "Nonlocal patch tensor sparse representation for hyperspectral image super-resolution," *IEEE Transactions on Image Processing*, vol. 28, no. 6, pp. 3034–3047, 2019.
- [33] Y. Peng, W. Li, X. Luo, and J. Du, "Hyperspectral image superresolution using global gradient sparse and nonlocal low-rank tensor decomposition with hyper-laplacian prior," *IEEE Journal of Selected Topics in Applied Earth Observations and Remote Sensing*, vol. 14, pp. 5453–5469, 2021.
- [34] S. Wang, T. Zhou, Y. Lu, and H. Di, "Contextual transformation network for lightweight remote sensing image super-resolution," *IEEE Transactions on Geoscience and Remote Sensing*, 2021.
- [35] F. Yasuma, T. Mitsunaga, D. Iso, and S. K. Nayar, "Generalized assorted pixel camera: postcapture control of resolution, dynamic range, and spectrum," *IEEE transactions on image processing*, vol. 19, no. 9, pp. 2241–2253, 2010.
- [36] A. Chakrabarti and T. Zickler, "Statistics of Real-World Hyperspectral Images," in *Proc. IEEE Conf. on Computer Vision and Pattern Recognition (CVPR)*, 2011, pp. 193–200.
- [37] N. Yokoya and A. Iwasaki, "Airborne hyperspectral data over chikusei," Space Application Laboratory, University of Tokyo, Japan, Tech. Rep. SAL-2016-05-27, May 2016. [Online]. Available: <http://park.itc.u-tokyo.ac.jp/sal/hyperdata/TechRepSAL20160527.pdf>
- [38] D. P. Kingma and J. Ba, "Adam: A method for stochastic optimization," *arXiv preprint arXiv:1412.6980*, 2014.
- [39] L. Loncan, L. B. De Almeida, J. M. Bioucas-Dias, X. Briottet, J. Chanussot, N. Dobigeon, S. Fabre, W. Liao, G. A. Licciardi, M. Simoes *et al.*, "Hyperspectral pansharpening: A review," *IEEE Geoscience and remote sensing magazine*, vol. 3, no. 3, pp. 27–46, 2015.
- [40] R. H. Yuhas, A. F. Goetz, and J. W. Boardman, "Discrimination among semi-arid landscape endmembers using the spectral angle mapper (sam) algorithm," in *Proc. Summaries 3rd Annu. JPL Airborne Geosci. Workshop*, vol. 1, 1992, pp. 147–149.
- [41] L. Wald, *Data fusion: definitions and architectures: fusion of images of different spatial resolutions*. Presses des MINES, 2002.
- [42] Z. Wang, A. C. Bovik, H. R. Sheikh, and E. P. Simoncelli, "Image quality assessment: from error visibility to structural similarity," *IEEE transactions on image processing*, vol. 13, no. 4, pp. 600–612, 2004.
- [43] J. Kim, J. Kwon Lee, and K. Mu Lee, "Accurate image super-resolution using very deep convolutional networks," in *Proceedings of the IEEE conference on computer vision and pattern recognition*, 2016, pp. 1646–1654.
- [44] Y. Zhang, K. Li, K. Li, L. Wang, B. Zhong, and Y. Fu, "Image super-resolution using very deep residual channel attention networks," in *Proceedings of the European conference on computer vision (ECCV)*, 2018, pp. 286–301.